

Anticipating and inoculating against hacks that exploit the emergent collective motion of autonomous vehicles

Skanda Vivek,^{1,*} David Yanni,^{1,†} Peter J. Yunker,^{1,‡} and Jesse L. Silverberg^{2,3,§}

¹*School of Physics, Georgia Institute of Technology, Atlanta, GA 30332*

²*Wyss Institute for Biologically Inspired Engineering, Harvard University, Boston, MA, 02115*

³*Department of Systems Biology, Harvard Medical School, Boston, MA 02115*

Recent events highlight the widespread risks malicious hacking poses to a modern internet-connected society. As automotive vehicles increase their level of computerized sophistication, they have become, and will continue to be, targets of opportunity. Here, we study how the beneficial emergent collective motion of autonomous vehicles can be weaponized and offer strategies to preemptively inoculate against this attack. Our approach combines empirical measurements with simulations of an active matter model to demonstrate that autonomous vehicles enhance traffic throughput, and that a relatively unsophisticated attack can have disproportionately negative consequences.

Autonomous self-driving vehicles are slated to bring substantial transformation to the automotive industry with foreseeable ripple effects in commercial and private sectors[1] [see SM]. These disruptions stem from the ability of autonomous vehicles to sense and rapidly respond to their environment. Inevitably, however, the software enabling these functions has a greater “surface area” for weakness to be exploited. As the recent public disclosure of stockpiled NSA hacking tools[2] and the subsequent global-scale ransomware attacks show[3, 4], software exploits can be weaponized by malicious actors. Already, proof-of-concept hacks in 2015 and 2016 have demonstrated the ability to remotely control the brakes, acceleration, steering, transmission, locks, stereo, and windshield wipers of a targeted vehicle by exploiting weaknesses including the internet-connected entertainment console[5, 6]. While attacks narrowly aimed at individual vehicles will continue to occur, another class of hacks that weaponizes emergent collective motion appears just as inevitable [see SM]. Fortunately, the physics of active matter[7, 8] offers a framework for understanding how collective motion can be weaponized without knowing the details of a specific software exploit *a priori*.

Here, we study the emergent collective motion of human and autonomously-driven vehicles. We first focus on the benefits of autonomous driving where fast reaction times and uniform driving speeds enable smooth traffic flow, even at high densities. Just as “white hat” hackers work to proactively identify software vulnerabilities, we shift our attention to study how immobilized hacked vehicles disrupt traffic. While the collective motion of autonomous vehicles that comes from their uniformity is beneficial, a malicious attack can lead to the undesirable emergence of obstructed flow.

From the various approaches used to study vehicular collective motion[9–15], we chose a force-based model[16,

17] that represents each vehicle by their position x at time t on a straight road of length L . Numerical simulations were performed using velocity Verlet integration for N vehicles seeded with uniformly distributed random initial positions, zero initial velocity, zero initial acceleration, and periodic boundary conditions. The position of each vehicle was evolved using a self-propulsion force $F^{\text{propulsion}}$, and a repulsive collision-avoidance force $F^{\text{repulsion}}$ according to

$$\begin{aligned}\ddot{x} &= F^{\text{propulsion}} + F^{\text{repulsion}}, \\ F^{\text{propulsion}} &= \tau_\alpha^{-1}(v_\alpha - \dot{x}), \\ F^{\text{repulsion}} &= \begin{cases} \epsilon_\alpha (1 - \delta x/R)^{3/2}, & \delta x < R \\ 0, & \text{otherwise} \end{cases} \quad (1)\end{aligned}$$

where \dot{x} and \ddot{x} are the velocity and acceleration of a given vehicle [see SM]. Each vehicle has a preferred speed v_α and a characteristic response time τ_α that it takes to equilibrate to this speed; in the absence of other vehicles, $F^{\text{repulsion}} \equiv 0$ and direct integration shows $\dot{x}(t) = v_\alpha(1 - e^{-t/\tau_\alpha})$. When the number of vehicles $N > 1$, the repulsive force acts to slow a given vehicle as it approaches another vehicle from behind. The strength of this force increases from zero as the vehicle-vehicle separation δx becomes smaller than the interaction threshold distance $R = v_\alpha \cdot (2 \text{ s})$. This threshold reflects the 2-second rule, which states that a minimum safe distance between two vehicles is the distance traveled during 2 seconds. The functional form of the repulsion force follows from the compression of two elastic spheres[18], and only applies to the trailing vehicle, as drivers respond to traffic ahead of them more strongly than behind. Given $F^{\text{repulsion}}$ is finite for all δx , this term is numerically stable in multi-vehicle simulations. However, the finite magnitude requires we fix the coefficient ϵ_α in terms of other variables so that the maximum propulsion force does not lead to unphysical effects such as one vehicle passing through another. Balancing propulsion and repulsion forces when two vehicles are bumper-to-bumper, we set $\delta x = r \equiv 4.5 \text{ m}$ as the typical size of a vehicle and find $\epsilon_\alpha \equiv (v_\alpha/\tau_\alpha)(1 - r/R)^{-3/2}$.

We focus on the emergent collective motion of two types of vehicles: human-driven and fully autonomous.

* skanda.vivek@physics.gatech.edu

† dyanni3@gatech.edu

‡ peter.yunker@gatech.edu

§ jesse.silverberg@wyss.harvard.edu

In Eq. (1), this simplification amounts to distinct values for the variables with subscript α , where we use $\alpha = H$ for human-driven vehicles and $\alpha = A$ for autonomous vehicles. For each of the N_H human drivers, we draw their preferred velocity v_H from a Gaussian distribution with mean 29 m/s (65 mi/h) and standard deviation 6.7 m/s (15 mi/h), approximating typical highway conditions. The only remaining free parameter in the equations of motion for human-driven vehicles is the response time τ_H , which generally varies from 0.5 s to several seconds, depending on attentiveness, age, driving conditions, visibility, and level of distractions. To empirically measure τ_H , we analyzed three sources of driving data including (i) a highway web cam in the San Francisco/Oakland Bay, California area (northbound 101 at N 1st street) [Fig. 1(a)][19], (ii) digital footage we filmed in Atlanta, Georgia (southbound I85 exit 249C) [Fig. 1(b)], and (iii) previously published Department of Transportation (DOT) traffic data from Los Angeles, California (southbound US 101; NGSIM June 15, 2005, 7:50 to 8:05 am)[20–22]. While the DOT data provided vehicle coordinates $x(t)$, we used quantitative image analysis on the first two video sources to obtain this information [see SM]. Differentiating and smoothing with a Savitzky-Golay filter allowed us to identify vehicles that stopped and accelerated over a time $t_f \approx 2 - 5$ s due to stop-and-go traffic. Assuming the repulsion force is negligible during the “go” phase, we fit this segment of the velocity data from each vehicle using non-linear least squares to the functional form $\dot{x}(0)/\dot{x}(t_f) = 1 - e^{-t/\tau_H}$ resulting in measurements of τ_H [Fig. 1(c)]. In high-density traffic, we observed drivers tend to accelerate over longer periods of time, whereas in low-density traffic, drivers tend to react faster. Because Eq. (1) simplifies driver response time to be density-independent, we perform a weighted average of the empirical measurements to set $\tau_H = 0.77$ s [see SM], which is $\approx 3\times$ the typical human reaction time to visual stimulus, and reasonably models attentive drivers.

In simulations of an $\ell = 1$ lane road, $L = 1.6$ km long, and with $N_H = 75$ human-driven vehicles, we find a brief transient ≈ 500 integration time steps followed by steady-state dynamics. Consistent with our empirical observations [see SM], we subsequently observed backwards-propagating density waves superimposed on the 1D line of traffic. These density waves cause stop-and-go motion of individual vehicles, and are otherwise known as “phantom traffic jams.” This emergent collective phenomenon has been extensively studied[9–14], and is generally understood as arising from a finite driver response time.

To perform multi-lane simulations, we require a model for lane-switching behavior. Currently, our only source of stochasticity in the steady-state dynamics are the N_H random velocities v_H . To preserve this feature of the model, we use a deterministic force-based approach where each vehicle is in a lane \mathcal{Y} that takes discrete values (e.g. 1, 2, 3, ...). The evolution of \mathcal{Y} for each vehicle is calculated by $\mathcal{Y}(t) = \text{round}[y(t)]$, where $y(t)$ is the equation for an overdamped oscillator driven by a force

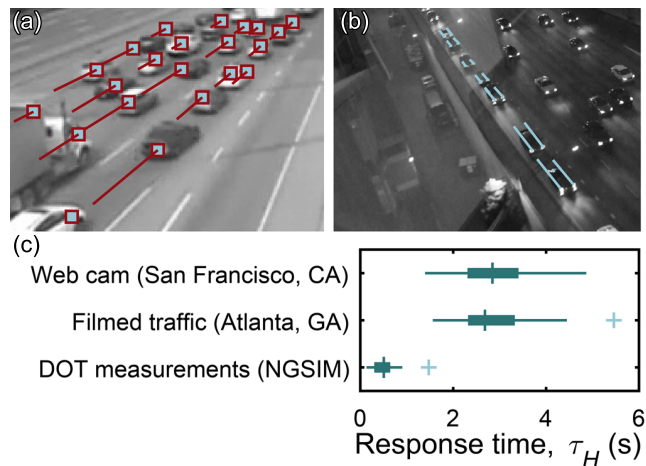


FIG. 1. Empirical measurements of a human-driven vehicle’s response time τ_H . (a) A live streamed web cam provides daytime data on traffic flow. Individual vehicles (squares) and their trajectories (lines) illustrate measurements of $x(t)$. (b) Nighttime highway traffic was filmed and analyzed using the same methods. (c) Fitting velocities during stop-and-go motion allows for measurements of the human-driver response time τ_H . Box-and-whisker plots show the median value, data quartiles, and outliers (+).

with magnitude $\propto (v_H - \dot{x})$ [see SM]. This *ad hoc* model for lane switching leads to stable lane preferences with vehicles traveling together at similar speeds, and self-sorting so that faster drivers switch lanes to bypass slower drivers. We fixed all parameters governing the dynamics of \mathcal{Y} at values that reproduce familiar phenomenology and validated our approach by comparing simulated and empirical density-dependent speed distributions [see SM].

Beyond qualitative observations of phantom traffic jams, the density-dependent flux $\Phi(\rho)$ is a useful quantity to study emergent collective properties of traffic flow [Fig. 2]. In empirical measurements and simulations with $\ell = 3$ lanes, we use a portion of the road $l \approx 500$ m to calculate $\Phi = \sum_i \dot{x}_i / (l\ell)$ and $\rho = \sum_i 1 / (l\ell)$, where the index i runs over all vehicles in l sampled at statistically independent temporal intervals. When the density is low, $\Phi \propto \rho$ [Fig. 2, $\rho < 40$ cars/km/lane]. As the density increases to a critical value $\rho^* \approx 40$ cars/km/lane, the flux peaks, and subsequently declines for increasing ρ . Both in empirical measurements and simulations, we find ρ^* corresponds to an average of one car per 25 m of road per lane. This distance is ≈ 1 s of travel time between vehicles, which places them well-within the repulsive-force interaction distance R . As such, when $\rho > \rho^*$, the system effectively becomes a 1D continuum with density waves (phantom traffic jams), and hence Φ declines.

Turning to self-driving vehicles, we model each of the N_A autonomous drivers by fixing their preferred velocity $v_A = 29$ m/s to be constant and equal to the typical speed limit (65 mi/hr). This reflects the notion that autonomous vehicles will be engineered to travel at the legally allowed maximum speed to optimize traf-

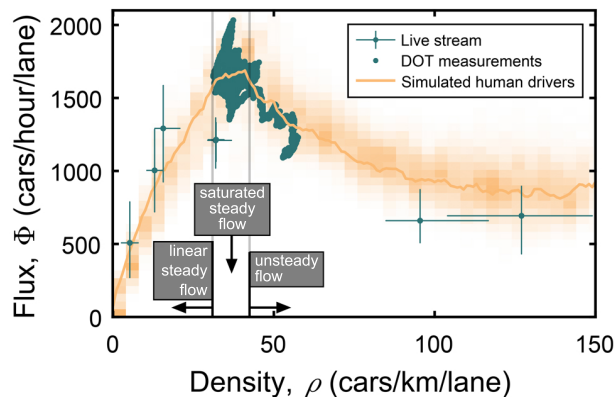


FIG. 2. Flux-density relationship for human-driven vehicles shows favorable agreement between empirical and simulation results. Error bars on live stream data are the inter-quartile range. DOT measurements are plotted as a continuous series of points near the critical density $\rho^* \approx 40$ cars/km/lane. Solid line is the simulated mean value of $\Phi(\rho)$ and the shaded band are statistical fluctuations.

fic flow. We also expect autonomous vehicles to utilize a combination of local sensor information, wirelessly shared non-local traffic conditions, and cloud-connected AI to respond to driving conditions more rapidly than human drivers. As an order of magnitude estimate, we set the autonomous vehicle response time $\tau_A = \tau_H/10$. Thus, the only difference between human-driven and autonomous vehicles in this active matter model are (i) response time τ_α and (ii) preferred speed v_α . Simulations with all autonomous vehicles immediately show important differences in the flux, highlighting a key advantage of autonomous driving [Fig. 3]. Specifically, $\Phi(\rho)$ still peaks near the same critical density ρ^* , however, the subsequent decrease in flux associated with phantom traffic jams essentially vanishes and instead declines a modest $\approx 10\%$ with a 4-fold increase in density [Fig. 3, upper dark line]. This trend is a significant improvement compared to human-driven vehicles where empirical observations and simulations show $\approx 50\%$ loss in flux over the same range in ρ [Fig. 2]. Interestingly, $\Phi(\rho)$ in all-autonomous vehicle simulations can be predicted from Eq. (1). Given the uniform preferred speed and rapid response time, $\Phi \approx N_A \dot{x}/(\ell L) = \rho \dot{x}$. Under steady conditions, propulsion and repulsion forces balance so that $\ddot{x} = 0$ and $\delta x = 1/\rho$, which leads to $\dot{x} = v_A - \tau \epsilon_A [1 - 1/(2\rho v_A)]^{3/2}$. The flux is therefore the real part of $\Phi(\rho) = \rho v_A - \rho \tau \epsilon_A [1 - 1/(2\rho v_A)]^{3/2}$, in agreement with simulations [Fig. 3, dashed line]. Substituting ϵ_A shows $\Phi(\rho)$ is independent of τ_A in the limit of uniformly distributed autonomous vehicles.

Given that autonomous vehicles *can* be hacked, it seems self-evident they *will* be hacked. Our goal is to look beyond the specifics of a given exploit, and to anticipate how autonomous vehicles can be weaponized. One possibility is that hacked vehicles are critically disabled causing them to become immobile obstacles on the road.

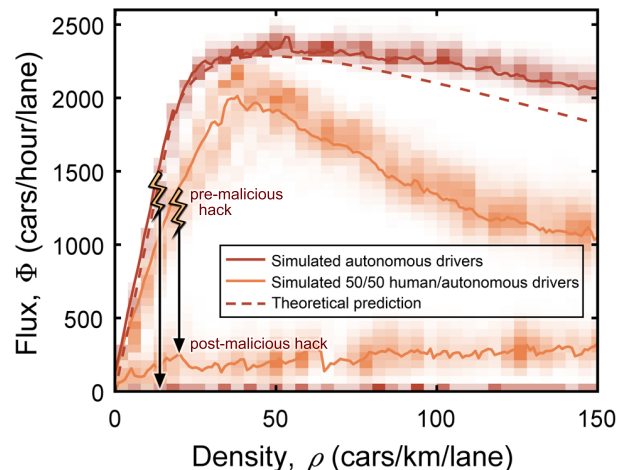


FIG. 3. Flux-density relationship for autonomously-driven vehicles shows how the benefits of increased traffic flow (upper curves) can be suppressed by a malicious hack (lower curves), effectively weaponizing vehicle collective motion. Simulations are for an all-autonomous fleet (dark curves) and a 50/50 mixed fleet of human and autonomous drivers (light curves). Dashed line is a fit-free theoretical prediction for $\Phi(\rho)$.

This type of “bricking” attack would cause significant social harm: emergency vehicles would be unable to respond to calls for help, food shipments to grocery stores would be delayed, and long-distance commuters would be unable to get to work. Urban cores and suburban towns, which are key centers of economic activity, would cease to function normally. Relative to its unsophisticated nature, a bricking attack would have disproportionate effects. Within the context of our active matter model, bricking amounts to setting $v_A = 0$, and the subsequent collective properties can be understood through measurements of $\Phi(\rho)$. In the case of an all autonomous fleet, the net flux simply goes to zero for all ρ [Fig. 3, lower dark line]. However, even with equal numbers of human and autonomous vehicles, the flux is dramatically suppressed [Fig. 3, lower light line]. Essentially, the malicious hack causes the N_A autonomous vehicles to become irregularly spaced obstacles clogging[15, 23] the road, and obstructing flow of the remaining N_H human-driven vehicles.

For a more complete view of how the flux is affected by malicious hacks, we treat Φ as an order parameter and generate the phase diagram composed of vehicle density ρ and the fraction of autonomously driven vehicles $N_A/(N_A + N_H)$ [Fig. 4(a)]. As expected from the simulations of all human, all autonomous, and 50/50 human/autonomous drivers, the phase diagram pre-malicious hack has three regions corresponding to linear steady flow ($\Phi \propto \rho$), a saturated steady flow where Φ is maximized and weakly dependent on ρ , and an unsteady flow regime where density waves decrease Φ . Post-malicious hack, the phase diagram collapses with unsteady and near-zero flow dominating while saturated steady flow appears at very low densities of

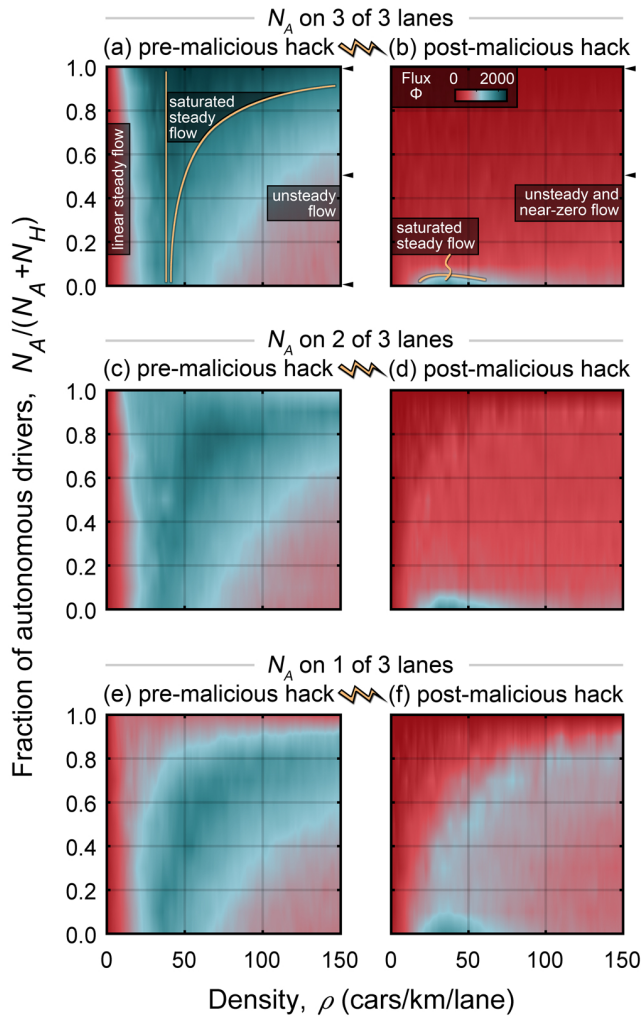


FIG. 4. Anticipating-and-inoculating against malicious hacks that weaponize autonomous vehicle collective motion. These phase diagrams for the flux order parameter Φ show how traffic is affected when autonomous vehicles are disabled, severely obstructing flow of un-hacked human-driven vehicles. (a) Benefits from autonomous vehicles are in the regime where traffic saturates and steadily flows. (b) Disabled autonomous vehicles create obstacles on the road generating unsteady and near-zero flow. (c) Restricting autonomous vehicles to 2 of the 3 available lanes leaves an unobstructed lane for human drivers in the event of a malicious hack, reducing the benefits of autonomous vehicles, but (d) allowing for modest flow. (e) Restriction of autonomous vehicles to 1 lane further reduces the benefits of autonomous vehicles but (f) strongly mitigates the consequences of a malicious hack. Right-most arrow heads in (a) and (b) along the axis edge point to cuts of the phase diagram plotted in Figs. 2 and 3.

autonomously-driven vehicles [Fig. 4(b)]. These differences between the pre- and post-hack phase diagrams show collective motion, or rather, the *lack* of collective motion, has significant disruptive potential.

A remarkable feature of the post-malicious hack phase diagram is the relatively low fraction of autonomous ve-

hicles required for traffic to be appreciably disrupted [Fig. 4(b), boundary between steady and unsteady flow]. In fact, this feature is surprisingly general and can be understood from combinatorial counting arguments [see SM]. Approximating the continuous road of length L as a discrete grid with dimensions $(L/r) \times \ell$, we randomly select N_A grid sites to be occupied by bricked autonomous vehicles. Traffic is stopped if ℓ vehicles are randomly assigned side-by-side positions, causing a blockage across all ℓ lanes. For $\ell = 2$, the probability of at least one blockage occurring when $\ell \ll L$ is $1 - (1 - \rho_A r)^{\rho_A L}$, which is one minus the probability of no blockages occurring, and $\rho_A = N_A/\ell L = N_A/2L$. Using the same $L = 1.6$ km road from simulations, the probability of traffic being completely stopped by a malicious bricking hack is 50% for $\rho_A \approx 16$ cars/km/lane, and 99% when $\rho_A \approx 40$ cars/km/lane. An analogous calculation for $\ell = 3$ shows the probabilities are 50% and 99% for $\rho_A \approx 45$ and 87 cars/km/lane, respectively. As such, vehicle densities well-within the range of empirical observations [Fig. 2, green data] have a substantial chance of completely obstructed flow post-malicious hack. These counting arguments help ground our understanding of the phase diagram [Fig. 4(b)], and ultimately suggest the physics of clogging[15, 23], random pinning in glasses[24, 25], and percolation[26, 27] may offer useful insights.

Anticipating how emergent collective motion can be weaponized ultimately suggests how to inoculate against this type of attack. One solution is to guarantee the existence of an unobstructed route for human drivers by limiting the N_A autonomous vehicles to a subset of lanes. Running simulations where human-driven vehicles were allowed on three lanes, but autonomously-driven vehicles were allowed on only two [Fig. 4(c-d)] or one [Fig. 4(e-f)] shows that benefits from autonomously driven vehicles can be retained while limiting the effects of a bricking attack, albeit with reduced flow rates [see SM].

By removing human variances in driving behavior, the collective motion of autonomous vehicles produces smooth, steady flowing traffic. This emergent property is highly desired for its environmental benefits, shortened commute times, and lower accident rates. Nevertheless, new technological achievements bring new potential risks. By disabling autonomous vehicles, malicious hackers can suppress this desirable collective motion leaving behind the highly disrupted collective motion of human drivers navigating in and around obstacles. As a bi-disperse active matter model, this situation leads to connections in the physics of clogging, random pinning, and percolation. Additionally, the absence of phantom traffic jams in the flow of autonomous vehicles suggests measurements of the dispersion relation and density of states may be useful probes to study the cross-over from human-driven to autonomously-driven vehicles. Working on these questions through the lens of the anticipate-and-inoculate mindset used here has the potential to identify how other emergent collective phenomena can be weaponized and preemptive disarmed. Ultimately, this approach should lead to safer roads and a greater good.

ACKNOWLEDGMENTS

The authors thank Zohar Nussinov for useful discussions and Christopher Giottonini for assistance with video acquisition. SV, DY, and PJY acknowledge support from the Georgia Tech Soft Matter Incubator. JLS was independently funded.

-
- [1] Todd Litman. Autonomous vehicle implementation predictions. *Victoria Transport Policy Institute*, 28, 2014.
 - [2] Robert Siegel. Shadow brokers group leaks stolen national security agency hacking tools, 2017. <http://www.npr.org/2017/06/29/534916031/shadow-brokers-group-leaks-stolen-national-security-agency-hacking-tools> [Online; accessed 2-August-2017].
 - [3] Bill Chappell. Wannacry ransomware: What we know monday, 2017. <http://www.npr.org/sections/thetwo-way/2017/05/15/528451534/wannacry-ransomware-what-we-know-monday> [Online; accessed 2-August-2017].
 - [4] Bill Chappell and Maggie Penman. Ransomware attacks ravage computer networks in dozens of countries, 2017. <http://www.npr.org/sections/thetwo-way/2017/05/12/528119808/large-cyber-attack-hits-englands-nhs-hospital-system-ransoms-demanded> [Online; accessed 2-August-2017].
 - [5] Andy Greenberg. Hackers remotely kill a jeep on the highway – with me in it, 2015. <https://www.wired.com/2015/07/hackers-remotely-kill-jeep-highway> [Online; accessed 2-August-2017].
 - [6] Andy Greenberg. The jeep hackers are back to prove car hacking can get much worse, 2016. <https://www.wired.com/2016/08/jeep-hackers-return-high-speed-steering-acceleration-hacks> [Online; accessed 2-August-2017].
 - [7] Sriram Ramaswamy. The mechanics and statistics of active matter. *The Annual Review of Condensed Matter Physics*, 1:323–45, 2010.
 - [8] M Cristina Marchetti, JF Joanny, S Ramaswamy, TB Liverpool, J Prost, Madan Rao, and R Aditi Simha. Hydrodynamics of soft active matter. *Reviews of Modern Physics*, 85(3):1143, 2013.
 - [9] Dirk Helbing. Traffic and related self-driven many-particle systems. *Reviews of Modern Physics*, 73:1067–1141, Dec 2001.
 - [10] Martin Treiber and Arne Kesting. Traffic flow dynamics. *Traffic Flow Dynamics: Data, Models and Simulation*, Springer-Verlag Berlin Heidelberg, 2013.
 - [11] M. J. Lighthill and G. B. Whitham. On kinematic waves. ii. a theory of traffic flow on long crowded roads. *Proceedings of the Royal Society of London A: Mathematical, Physical and Engineering Sciences*, 229(1178):317–345, 1955.
 - [12] Gordon Frank Newell. A simplified car-following theory: a lower order model. *Transportation Research Part B: Methodological*, 36(3):195–205, 2002.
 - [13] Martin Treiber, Ansgar Hennecke, and Dirk Helbing. Congested traffic states in empirical observations and microscopic simulations. *Physical Review E*, 62(2):1805, 2000.
 - [14] Kai Nagel and Michael Schreckenberg. A cellular automaton model for freeway traffic. *Journal de Physique I*, 2(12):2221–2229, 1992.
 - [15] Takashi Nagatani. The physics of traffic jams. *Reports on Progress in Physics*, 65(9):1331, 2002.
 - [16] Jesse L Silverberg, Matthew Bierbaum, James P Sethna, and Itai Cohen. Collective motion of humans in mosh and circle pits at heavy metal concerts. *Physical Review Letters*, 110(22):228701, 2013.
 - [17] Arianna Bottinelli, David TJ Sumpter, and Jesse L Silverberg. Emergent structural mechanisms for high-density collective motion inspired by human crowds. *Physical Review Letters*, 117(22):228301, 2016.
 - [18] Lev Davidovich Landau and Eugin M Lifshitz. *Course of Theoretical Physics Vol 7: Theory and Elasticity*. Pergamon Press, 1959.
 - [19] <http://www.dot.ca.gov/video/index.html>.
 - [20] United States Department of Transportation Federal High Administration. Ngsim datasets, 2005. <https://www.its-rde.net/index.php/rdedataenvironment/10023> [Online; accessed 2-August-2017].
 - [21] Vassili Alexiadis, James Colyar, and John Halkias. A model endeavor. *Public Roads*, 70(4), 2007.
 - [22] Marcello Montanino and Vincenzo Punzo. Making ngsim data usable for studies on traffic flow theory: Multistep method for vehicle trajectory reconstruction. *Transportation Research Record: Journal of the Transportation Research Board*, 2390:99–111, 2013.
 - [23] Cesare Mikhail Cejas, Fabrice Monti, Marine Truchet, Jean-Pierre Burnouf, and Patrick Tabeling. Particle deposition kinetics of colloidal suspensions in microchannels at high ionic strength. *Langmuir*, 2017.
 - [24] Chiara Cammarota and Giulio Biroli. Ideal glass transitions by random pinning. *Proceedings of the National Academy of Sciences*, 109(23):8850–8855, 2012.
 - [25] Astrid S de Wijn, DM Miedema, B Nienhuis, and P Schall. Criticality in dynamic arrest: Correspondence between glasses and traffic. *Physical Review Letters*, 109(22):228001, 2012.
 - [26] Amnon Aharony and Dietrich Stauffer. *Introduction to percolation theory*. Taylor & Francis, 2003.
 - [27] Jesse L Silverberg. A model for conductive percolation in ordered nanowire arrays. *Journal of Applied Physics*, 105(4):044306, 2009.